

Tunable coupling of widely separated superconducting qubits: A possible application towards a modular quantum device

Peng Zhao,^{1,*} Yingshan Zhang,^{1,†} Guangming Xue,^{1,‡} Yirong Jin,¹ and Haifeng Yu¹

¹*Beijing Academy of Quantum Information Sciences, Beijing 100193, China*

(Dated: May 27, 2022)

Besides striving to assemble more and more qubits in a single monolithic quantum device, taking a modular design strategy may mitigate numerous engineering challenges for achieving large-scalable quantum processors with superconducting qubits. Nevertheless, a major challenge in the modular quantum device is how to realize high-fidelity entanglement operations on qubits housed in different modules while preserving the desired isolation between modules. In this work, we propose a conceptual design of a modular quantum device, where nearby modules are spatially separated by centimeters. In principle, each module can contain tens of superconducting qubits, and can be separately fabricated, characterized, packaged, and replaced. By introducing a bridge module between nearby qubit modules and taking the coupling scheme utilizing a tunable bus, tunable coupling of qubits that are housed in nearby qubit modules, could be realized. Given physically reasonable assumptions, we expect that sub-100-ns two-qubit gates for qubits housed in nearby modules which are spatially separated by more than two centimeters could be obtained. In this way, the inter-module gate operations are promising to be implemented with gate performance comparable with that of intra-module gate operations. Moreover, with help of through-silicon vias technologies, this long-range coupling scheme may also allow one to implement inter-module couplers in a multi-chip stacked processor. Thus, the tunable longer-range coupling scheme and the proposed modular architecture may provide a promising foundation for solving challenges toward large-scale quantum information processing with superconducting qubits.

I. INTRODUCTION

After sustained and intense effort in the improvement of qubit performance and functionality, quantum devices with tens of superconducting qubits have been realized. This has led to impressive achievements in superconducting quantum-information processing [1–3]. Nevertheless, the current small-scale noisy quantum processor is still insufficient to support the pursuit of quantum advantage (e.g., solving complex problems that are intractable for classical computing) for practical applications [4] and the long-term goal of fault-tolerant quantum computing [5, 6]. Thus, in addition to striving for further improvement of qubit performance, focus also begins to shift to the scaling of these small-scale quantum devices into large-scale quantum systems. Integrating an increasing number of qubits without sacrificing qubit performance, especially in monolithic quantum devices, requires overcoming several scientific and technical challenges, such as the wiring problem [7–9], crosstalk [10–12], and fabrication yield [13, 14]. To overcome these limitations, various schemes have been proposed and demonstrated, such as the compact integration of quantum devices with the classical cryogenic control systems [15–19], the three-dimensional (3D) integration technologies [20–25], and the post-processing of the fabricated qubit devices [26–28].

From a system integration perspective, building large quantum systems out of smaller modules may mitigate various challenges faced by the monolithic integration strategy [17, 29–32]. As in modular devices incorporating several mod-

ules, each module can be separately fabricated, characterized, and replaced. Thus, the fabrication yield of the large modular system can be improved, and the electromagnetic crosstalk or impact of some correlated errors, such as caused by the high energy background radiation [33–35], may be restricted to the module scale. In addition, for modular devices with larger spatial separation between modules, the vacant space between modules could be employed to increase the control footprint area for qubit control, and could even be used to integrate on-chip control electronics [15, 17, 19, 36]. This allows for a more-compact integration of the qubit device and its classical control system, thus potentially mitigating the wiring problem [7, 8]. Despite these appealing features, there is a major challenge in modular quantum devices, i.e., how to realize fast-speed, high-fidelity entanglement operations across qubits housed in different modules while keeping adequate physical isolation between modules.

For multiqubit quantum processors, to ensure high-fidelity gate operations, qubits are generally coupled via a coupler circuit [37–40], which is employed to mitigate various quantum crosstalks due to parasitic couplings, such as ZZ crosstalk [40]. In this way, the entanglement gate operations are generally implemented with short-ranged couplings, limiting the spatial distance between coupled qubits to a few millimeters. In principle, by using these short-range coupling schemes, inter-module gate operations can be implemented with performance comparable with that of the intra-module gate operation [32]. However, in an ideal modular device, this short-ranged coupling between inter-module qubits is not compatible with the pursuit of the desired physical isolation between modules.

In this work, we propose a conceptual design of a modular quantum device, where inter-module qubits are coupled via a bridge module. The inter-module coupling scheme is a natural extension of a previously proposed scheme utilizing a

*Electronic address: shangniguo@sina.com

†Electronic address: zhangys@baqis.ac.cn

‡Electronic address: xuegm@baqis.ac.cn

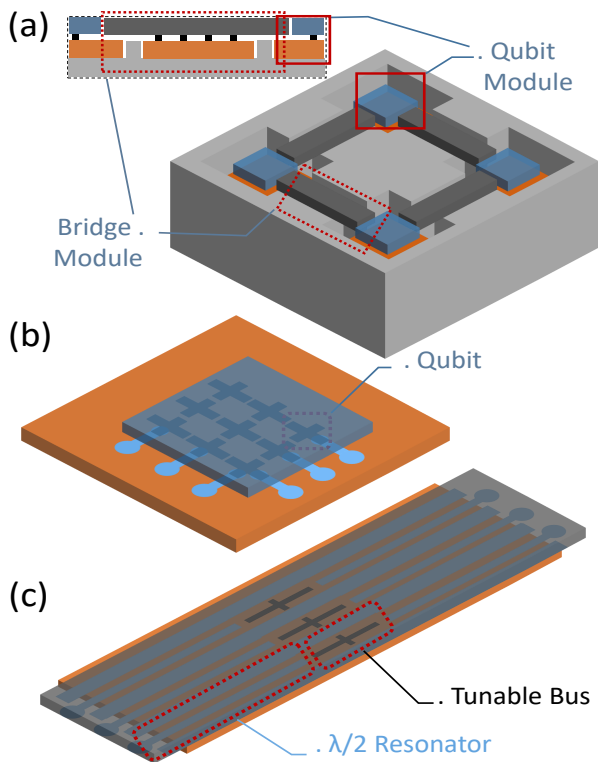


FIG. 1: Conceptual schematic of a possible modular quantum device utilizing bump-bonding technologies (not to scale). (a) The modular device comprises two types of functional modules: qubit modules and bridge modules. Before assembly, each module can be separately fabricated, packaged, and characterized. After chip assembly and test, damaged modules due to junction aging of qubits can also be replaced. The inset (outlined with the black dashed box) shows the cross-sectional view of the modular device. (b) As in traditional monolithic devices utilizing bump-bonding technologies [22, 24], each qubit module can contain tens of qubits (hosted on the top chip, grey) and their ancillary circuits (patterned on the carrier chip, orange) for qubit operations. Here, for example, each qubit module contains a 3×3 qubit lattice. (c) The bridge modules are introduced to mediate coupling between qubits residing in nearby qubit modules, thus allowing for intra-module entanglement gate operations. The plot presented here shows that each bridge module comprises three coupler circuits, which are used to mediate inter-qubit coupling between qubits external to each qubit module. The coupler circuit consists of two $\lambda/2$ CPW resonators which are interconnected by a tunable bus, and all three elements are hosted on the top chip (grey).

tunable bus [41], which can be employed for suppressing parasitic interactions and implementing sub-100-ns Controlled-Z (CZ) gates for inter-module qubits. Given physical assumptions, we expect that tunable coupling (entanglement gate operations) of qubits housed in nearby qubit modules, and which are spatially separated by more than two centimeters could be obtained. Thus, here, it is promising to implement high-fidelity inter-module gate operations while maintaining the desired physical isolation between modules.

II. OVERVIEW OF A MODULAR SUPERCONDUCTING QUANTUM PROCESSOR

As sketched in Fig. 1(a), we consider a modular quantum device comprising two types of functional module: qubit modules and bridge modules. In principle, before the device assembly, each module can be separately fabricated, packaged, and characterized. Therefore, only the modules which function properly during the test, are assembled into the modular device. This could improve the fabrication yield of the large modular system.

In addition, after device assembly, damaged modules can arise, such as due to junction aging of qubits [42–45]. The aging process is generally attributed to aluminum hydrates present in the junction barrier, which can result from fabrication residuals [43, 44]. Moreover, the non-uniformity present in qubit fabrication [46] could make the aging process differently over qubits and qubit modules. To improve the fabrication efficiency of modular devices, it is highly desirable to replace the damaged module while keeping minimal impacts on the performance of other functional modules. For this purpose, rather than taking bump-bonding or wire-bonding technologies for integrating the two-type modules, where qubit modules should have, e.g., galvanic connections, with bridge modules, one may prefer underfill technologies [17]. In this situation, all modules are underfilled to a chip mount or an additional large carrier chip, as shown in the inset of Fig. 1(a), and the coupler circuits housed on the bridge module are coupled capacitively to the qubits that reside in the qubit module. This makes it possible to have a modular device with replaceable modules. However, the underfill epoxies can induce dielectric loss, which should be minimized to avoid degradation of qubit coherence [17].

Similar to traditional monolithic quantum devices, each qubit module can contain tens of qubits and their ancillary circuits for qubit control, e.g., readout resonators for qubit measurement, and control lines for gate operations. Fig. 1(b) shows a typical qubit module utilizing bump-bonding technologies, where both qubits and their ancillary circuits can be fabricated by lithographically patterned superconducting metallization layer, e.g., aluminum, on high-quality substrates, e.g., high resistivity silicon substrates.

As the surface code scheme requires a two-dimensional (2D) lattice of qubits with only nearest-neighbor couplings [5], here, intra-module qubits can be coupled via the traditional short-range couplers, and inter-module qubits, i.e., qubits in the outer perimeter of each qubit module, can be coupled through the coupler circuits housed in bridge modules. Thus, the proposed modular architecture can be scaled up without any sacrifice of qubit connectivity. Moreover, the bridge module can decrease qubit density and create vacant space, thus increasing the control footprint area for qubit control and potentially mitigating the wire problem [36].

To couple inter-module qubits, we consider a bus-mediated longer-range coupling scheme. The scheme is an extension of the recently proposed coupling scheme [41], where two qubits are coupled via a bus, and tunable ZZ coupling can be achieved through tuning the bus frequency. In addition, weak

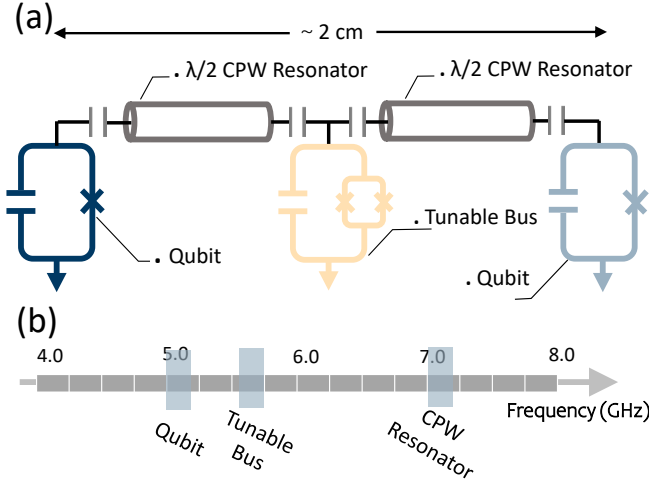


FIG. 2: Circuit schematic of the proposed coupler circuit for coupling qubits in nearby qubit modules (not to scale). (a) Two fixed-frequency transmon qubits, that are spatially separated by 2 cm, are coupled together via a coupler circuit. The circuit consists of two $\lambda/2$ resonators, which are interconnected via a frequency-tunable transmon qubit (acted as the tunable bus). (b) Frequency arrangement of the qubit and the coupler circuit (two resonators and one tunable bus). The qubit frequency is around 5.0 GHz, the bus idle frequency is typically 500 MHz above the qubit's, and the fundamental mode frequency of the resonator is about 7.0 GHz.

qubit-bus coupling, typically with a strength of 20 MHz, is adequate for implementing sub-100-ns CZ gates. Since strong interactions have been demonstrated for distant qubits coupled to a common half-wave superconducting coplanar waveguide resonator ($\lambda/2$ CPW resonator) [47, 48], resonator-mediated qubit-bus couplings with strengths of 20 MHz should be achieved. Thus, we expect that the coupler circuit, which consists of two $\lambda/2$ CPW resonators connected via a frequency-tunable transmon qubit (acted as a tunable bus), as shown in Fig. 1(c), should be a feasible longer-range coupler for realizing tunable ZZ coupling and implementing sub-100-ns CZ gates for inter-module qubits.

III. ENTANGLEMENT OPERATIONS ON QUBITS HOUSED IN NEARBY MODULES

Figure 2(a) shows the circuit schematic of a coupled two-qubit system, where two fixed-frequency transmon qubits [49] (housed in the nearby qubit modules) are coupled via the proposed coupler circuit (housed in the bridge module). The full system can be modeled by a chain of five modes including three anharmonic modes (two qubits and one tunable bus) and two harmonic modes (two resonators) with nearest-

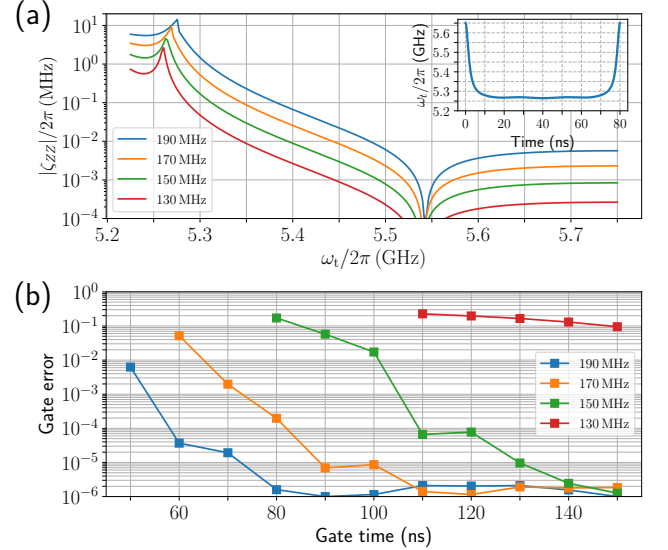


FIG. 3: Tunable ZZ coupling and its application for implementing two-qubit CZ gates. The parameters used here are: qubit frequency $\omega_{1(2)}/2\pi = 5.0(5.2)$ GHz, qubit (bus) anharmonicity $\eta_1 = \eta_2 = \eta_t = \eta$ with $\eta/2\pi = -300$ MHz, resonator frequency $\omega_{r1(r2)}/2\pi = 7.0(7.2)$ GHz, and resonator coupling strength $g_{tk} = g_{rk} = g$ (calculated at $\omega_i/2\pi = \omega_{rj}/2\pi = 6.0$ GHz) with $g/2\pi = \{130, 150, 170, 190\}$ MHz. (a) ZZ coupling strength ζ_{ZZ} as a function of the bus frequency ω_t for the coupled qubit system illustrated in Fig. 2(a). The inset shows the typical control pulse shape of the bus frequency for an 80-ns CZ gate, where the bus frequency is tuned from the idle point at 5.65 GHz to the working point near 5.27 GHz, and then coming back. (b) CZ gate errors versus gate time without the consideration of the system decoherence process.

neighboring coupling, described by (hereafter $\hbar = 1$)

$$\begin{aligned}
 H = & \sum_{i=1,2,t} \left(\omega_i a_i^\dagger a_i + \frac{\eta_i}{2} a_i^\dagger a_i^\dagger a_i a_i \right) + \sum_{j=1,2} \omega_{rj} b_j^\dagger b_j \\
 & + \sum_{k=1,2} g_{tk} (a_t^\dagger + a_t) (b_k + b_k^\dagger) \\
 & + \sum_{k=1,2} g_{rk} (a_k^\dagger + a_k) (b_k + b_k^\dagger),
 \end{aligned} \tag{1}$$

where the subscript i labels the anharmonic mode Q_i with anharmonicity η_i and bare mode frequency ω_i , and the subscript j labels the harmonic mode R_j with bare mode frequency ω_{rj} . a_i (a_i^\dagger) is the annihilation (creation) operator for the modes Q_i , and b_j (b_j^\dagger) is for modes R_j . g_{tk} (g_{rk}) denotes the coupling strength between the mode Q_t (Q_k) and the resonator R_k .

As shown in Fig. 2(b), here we consider that the qubit frequency is around 5.0 GHz, the bus idle frequency is typically 500 MHz above the qubit's, and the resonator frequency is about 7.0 GHz. Assuming that the dielectric constant of the substrate (silicon) is $\epsilon_r = 11.45$, the $\lambda/2$ CPW resonator with the length 9 mm has the fundamental mode at 7 GHz [50, 51]. As the typical size of the transmon qubit is about 1 mm [9], we

expect that coupling of qubits that are spatially separated by more than 2 cm can be realized. Thus, given this long-range coupling scheme, modular devices with large intra-module separation distance could be achieved, potentially enabling the desired physical isolation between qubit modules.

As mentioned earlier, here, the ZZ coupling of qubits can be controlled by adjusting the bus frequency. Fig. 3(a) show the ZZ coupling strength versus the bus frequency with different resonator coupling strength. Here, the ZZ coupling strength is defined as (hereafter, notation $|Q_1 R_1 Q_t R_2 Q_2\rangle$ denotes the full system state, and when confined to qubit subspace, notation $|Q_1 Q_2\rangle$ is used)

$$\zeta_{ZZ} \equiv (E_{11} - E_{10}) - (E_{01} - E_{00}), \quad (2)$$

and can be obtained numerically by diagonalizing the full system Hamiltonian in Eq. (1). In Eq. (2), E_{jk} denotes the eigenenergy of the full system associated with eigenstate $|jk\rangle$, which is adiabatically connected to the bare state $|j000k\rangle$ [52].

From the results shown in Fig. 3(a), one can find that the ZZ coupling can be suppressed below 10 kHz by tuning the bus frequency above 5.5 GHz, thus high-performance single-qubit control can be realized with ZZ -suppression. Furthermore, when the resonator coupling strength g takes values larger than 170 MHz, ZZ coupling with strength above 10 MHz can be achieved with the bus frequency near 5.27 GHz, thus sub-100-ns CZ gates should be obtainable. Here, we consider that the CZ gate is implemented by tuning the bus frequency according to a fast adiabatic control pulse [54]. The typical control pulse shape of the bus frequency can be found in the inset of Fig. 3(a), where the bus frequency is tuned from the idle point (at 5.65 GHz, where ZZ coupling is suppressed below 10 kHz) to the working point (near 5.27 GHz, where the ZZ coupling takes its maximum value, i.e., about 10 MHz), and then coming back. The detailed procedure for tuning up the fast-adiabatic CZ gate and characterizing the intrinsic CZ gate performance (i.e., in the absent of decoherence) can be found in Ref.[41].

To evaluate gate performance, Figure 3(b) shows the CZ gate error as a function of the gate time without the consideration of the system decoherence process [53]. One can find that with the resonator coupling strength above 170 MHz, high-fidelity sub-100-ns CZ gates can be achieved. This suggests that with this tunable coupling scheme, the inter-module gate operations are promising to be implemented with gate performance comparable with that of intra-module gate operations.

In practical implementations, compared with the original scheme, one may expect that besides the decoherence processes of the qubits and the bus, the difficulties to face with the present scheme depend on one additional limitation, i.e., the resonator decay process. Here, to study the influence of the resonator decay process on the CZ gate performance, the Lindblad master equation is employed. To be more specific, by considering the resonator decay process, the master equation can be expressed as

$$\frac{d\rho}{dt} = -i[H, \rho] + \sum_{j=1,2} \kappa_j \mathcal{L}[b_j], \quad (3)$$

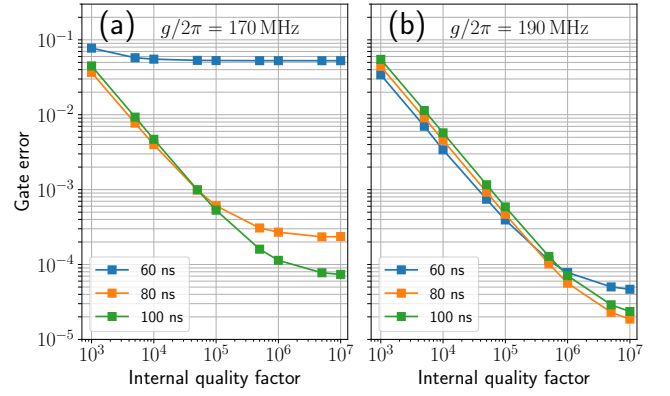


FIG. 4: CZ gate error versus the internal quality factor of the resonator. The resonator coupling strength is $g/2\pi = 170$ MHz for (a), and $g/2\pi = 190$ MHz for (b), and the decay rate of the resonator is $\kappa_j = \omega_{rj}/Q_j$ (here, the internal quality factors of the two resonators take the same value). The other system parameters are the same as in Fig. 3.

where the Hamiltonian H is given in Eq. (1), ρ is the density matrix of the system, $\mathcal{L}[b_j] = b_j \rho b_j^\dagger - b_j^\dagger b_j \rho / 2 - \rho b_j^\dagger b_j / 2$ describes the resonator decay terms, κ_j denotes the photon decay rate of resonator R_j . The average gate fidelity of the CZ gate under the resonator decay process is defined as [55]

$$F = \frac{dF_p + 1 - L_1}{d + 1}, \quad (4)$$

where d denotes the dimension of the computational subspace of the system, L_1 represents the leakage of the gate operation, and F_p is the process fidelity of the implemented CZ gate. The process fidelity F_p can be obtained by numerically performing quantum process tomography of the implemented CZ gate based on the master equation given in Eq. (3). Similarly, the leakage L_1 can be obtained by solving the master equation with the system initialized in different computational states [55].

Figure 4 shows the CZ gate error $1 - F$ versus the internal quality factor of the resonator. one can find that sub-100-ns CZ gates with gate errors below 0.01 (0.001) can be achieved with the resonator internal quality factor exceeding 5×10^3 (5×10^4). Given the state-of-the-art results, planar superconducting CPW resonators with internal quality factors above 10^6 have been demonstrated [56–58]. Therefore, the result shown in Fig. 4 suggests that with current technologies, the gate error from the resonator decay process is promising to be pushed below 0.001.

In addition, in the presence of decoherence, there generally exists two gate error channels, i.e., decoherence error due to the resonator decay and coherence error including leakage resulting from non-adiabatic transitions. The two channels favor opposite gate strategies, i.e., short gate times for mitigating decoherence error and longer gate times for suppressing coherence error. The tradeoff between the two types of error can explain that the gates with longer gate times do not always show better performance, as shown in Fig. 4. Moreover,

by comparing the results in Fig. 4(a) and 4(b), one can find that although larger resonator coupling can decrease the coherent error, as also shown in Fig. 3(b), it can, on the contrary, increase the decoherence error through the resonator decay process. This is to be expected, as larger resonator coupling can result in a strong state hybrid between the qubit and the resonator, thus qubit relaxation through the resonator can become more serious [38].

IV. DISCUSSION AND CONCLUSION

In summary, the work aims to show the possibility of solving challenges toward large-scale quantum devices with tunable longer-range coupling. We have shown that with the proposed tunable longer-range coupler, a modular quantum device with fast-speed, high-fidelity inter-module gate operations and desired physical isolation could be obtained. This could give rise to a promising foundation for mitigating several scientific and technical challenges toward large-scale superconducting quantum computing. Though, in practice, the feasibility of the proposed modular design may be limited because of several relevant engineering challenges, e.g., the assembly accuracy of modules [32], and the parasitic electromagnetic modes within the device package [10, 12], another goal of this work is to encourage further experimental and theoretical research in incorporating long-range inter-qubit cou-

pling into scalable quantum information processing with superconducting qubits [59].

While in the present work, the introduced longer-range coupler is employed for realizing longer-range tunable ZZ coupling and CZ gates, in the supplementary material, we further show that the coupler could also be used for implementing other types of two-qubit gate. We will show that by setting the bus frequency at 5.5 GHz, the ZZ coupling has been suppressed heavily, as shown in Fig. 3(a), meanwhile, the transversal (XY) coupling between qubits can still be maintained [60]. Thus, for qubits coupled via the proposed coupler, all-microwave-controlled cross-resonance gates (or CX gates) can be realized with ZZ suppression [61].

Acknowledgments

We would like to thank Xuegang Li and Junling Long for their helpful discussions and comments. Numerical analysis of the resonator decay process on gate performance were performed using the Quantum Toolbox in Python (QuTiP) [62]. This work was partly supported by the National Natural Science Foundation of China (Grants No.11890704, No.12004042), the Beijing Natural Science Foundation (Grant No.Z190012), and the Key-Area Research and Development Program of Guang Dong Province (Grant No. 2018B030326001).

-
- [1] F. Arute, K. Arya, R. Babbush, D. Bacon, J. C. Bardin, R. Barends, R. Biswas, S. Boixo, F. G. Brandao, D. A. Buell *et al.*, Quantum supremacy using a programmable superconducting processor, *Nature* **574**, 505 (2019).
 - [2] Q. Zhu, S. Cao, F. Chen, M.-C. Chen, X. Chen, T.-H. Chung, H. Deng, Y. Du, D. Fan, M. Gong *et al.*, Quantum computational advantage via 60-qubit 24-cycle random circuit sampling, *Science Bulletin* **67**, 240 (2022).
 - [3] P. Jurcevic, A. Javadi-Abhari, L. S. Bishop, I. Lauer, D. F. Bogorin, M. Brink, L. Capelluto, O. Günlük, T. Itoko, N. Kanazawa *et al.*, Demonstration of quantum volume 64 on a superconducting quantum computing system, *Quantum Sci. Technol.* **6**, 025020 (2021).
 - [4] J. Preskill, Quantum Computing in the NISQ era and beyond, *Quantum* **2**, 79 (2018).
 - [5] A. G. Fowler, M. Mariantoni, J. M. Martinis, and A. N. Cleland, Surface codes: Towards practical large-scale quantum computation, *Phys. Rev. A* **86**, 032324 (2012).
 - [6] J. M. Martinis, Qubit Metrology for Building a Fault Tolerant Quantum Computer, *npj Quantum Inf.* **1**, 15005 (2015).
 - [7] D. P. Franke, J. S. Clarke, L. M. K. Vandersypen, and M. Veldhorst, Rent's rule and extensibility in quantum computing, *Microprocess. Microsy.* **67**, 1 (2019).
 - [8] D. J. Reilly, Challenges in Scaling-up the Control Interface of a Quantum Computer, *2019 IEEE International Electron Devices Meeting (IEDM)*, 31.7 (2019).
 - [9] J. M. Martinis, Information Constraints for Scalable Control in a Quantum Computer, *arXiv:2012.14270*.
 - [10] J. Wenner, M. Neeley, R. C. Bialczak, M. Lenander, E. Lucero, A. D. ÓConnell, D. Sank, H. Wang, M. Weides, A. N. Cleland, and J. M. Martinis, Wirebond cross talk and cavity modes in large chip mounts for superconducting qubits, *Supercond. Sci. Technol.* **24**, 065001 (2011).
 - [11] R. Barends, J. Kelly, A. Megrant, A. Veitia, D. Sank, E. Jeffrey, T. C. White, J. Mutus, A. G. Fowler, B. Campbell *et al.*, Superconducting quantum circuits at the surface code threshold for fault tolerance, *Nature* **508**, 500 (2014).
 - [12] S. Huang, B. Lienhard, G. Calusine, A. Vepsäläinen, J. Braumüller, D. K. Kim, A. J. Melville, B. M. Niedzielski, J. L. Yoder, B. Kannan *et al.*, Microwave Package Design for Superconducting Quantum Processors, *PRX Quantum* **2**, 020306 (2021)
 - [13] J. M. Gambetta, J. M. Chow, and M. Steffen, Building logical qubits in a superconducting quantum computing system, *npj Quantum Inf.* **3**, 2 (2017).
 - [14] M. Brink, J. M. Chow, J. Hertzberg, E. Magesan, and Sami Rosenblatt, Device challenges for near term superconducting quantum processors: frequency collisions, *2018 IEEE International Electron Devices Meeting (IEDM)*, (2018).
 - [15] E. Leonard Jr., M. A. Beck, J. Nelson, B.G. Christensen, T. Thorbeck, C. Howington, A. Opremcak, I.V. Pechenezhskiy, K. Dodge, N.P. Dupuis *et al.*, Digital Coherent Control of a Superconducting Qubit, *Phys. Rev. Appl.* **11**, 014009 (2019).
 - [16] R. McDermott, M. G. Vavilov, B. L. T. Plourde, F. K. Wilhelm, P. J. Liebermann, O. A. Mukhanov and T. A. Ohki, Quantum-classical interface based on single flux quantum digital logic, *Quantum Sci. Technol.* **3**, 024004 (2018).
 - [17] R. N. Das, J. L. Yoder, D. Rosenberg, D. K. Kim, D. Yost, J. Mallek, D. Hover, V. Bolkhovskiy, A. J. Kerman, and W. D. Oliver, Cryogenic qubit integration for quantum computing,

2018 IEEE 68th Electronic Components and Technology Conference (ECTC), 504 (2018).

- [18] J. C. Bardin, E. Jeffrey, E. Lucero, T. Huang, S. Das, D. T. Sank, O. Naaman, A. E. Megrant, R. Barends, T. White *et al.*, Design and Characterization of a 28-nm Bulk-CMOS Cryogenic Quantum Controller Dissipating Less Than 2 mW at 3 K, *IEEE Journal of Solid-State Circuits* **54**, 3043 (2019).
- [19] A. Potočník, S. Brebels, J. Verjauw, R. Acharya, A. Grill, D. Wan, M. Mongillo, R. Li, T. Ivanov, S. V. Winckel *et al.*, Millikelvin temperature cryo-CMOS multiplexer for scalable quantum device characterisation, *Quantum Sci. Technol.* **7**, 015004 (2021).
- [20] J. H. Béjanin, T. G. McConkey, J. R. Rinehart, C. T. Earnest, C. R. H. McRae, D. Shiri, J. D. Bateman, Y. Rohanizadegan, B. Penava, P. Breul *et al.*, Three-Dimensional Wiring for Extensible Quantum Computing: The Quantum Socket, *Phys. Rev. Appl.* **6**, 044010 (2016).
- [21] Q. Liu, M. Li, K. Dai, K. Zhang, G. Xue, X. Tan, H. Yu, and Y. Yu, Extensible 3D architecture for superconducting quantum computing, *Appl. Phys. Lett.* **110**, 232602 (2017).
- [22] D. Rosenberg, D. Kim, R. Das, D. Yost, S. Gustavsson, D. Hover, P. Krantz, A. Melville, L. Racz, G. O. Samach *et al.*, 3D integrated superconducting qubits, *npj Quantum Inf.* **3**, 1 (2017).
- [23] N. T Bronn, V. P Adiga, S. B Olivadese, X. Wu, J. M Chow, and D. P Pappas, High coherence plane breaking packaging for superconducting qubits, *Quantum Sci. Technol.* **3**, 024007 (2018).
- [24] B. Foxen, J. Y. Mutus, E. Lucero, R. Graff, A. Megrant, Y. Chen, C. Quintana, B. Burkett, J. Kelly, E. Jeffrey *et al.*, Qubit compatible superconducting interconnects, *Quantum Sci. Technol.* **3**, 014005 (2018).
- [25] P. A. Spring, T. Tsunoda, B. Vlastakis, and P. J. Leek, Modeling Enclosures for Large-Scale Superconducting Quantum Circuits, *Phys. Rev. Appl.* **14**, 024061 (2020).
- [26] C. Granata, A. Vettoliere, L. Petti, M. Rippa, B. Ruggiero, P. Mormile, and M. Russo, Trimming of critical current in niobium Josephson devices by laser annealing, *J. Phys. Conf. Ser.* **97**, 012110 (2008).
- [27] J. B. Hertzberg, E. J. Zhang, S. Rosenblatt, E. Magesan, J. A. Smolin, J.-B. Yau, V. P. Adiga, M. Sandberg, M. Brink, J. M. Chow, and J. S. Orcutt, Laser-annealing Josephson junctions for yielding scaled-up superconducting quantum processors, *npj Quantum Inf.* **7**, 129 (2021).
- [28] M. Mergenthaler, C. Müller, M. Ganzhorn, S. Paredes, P. Müller, G. Salis, V.P. Adiga, M. Brink, M. Sandberg, J.B. Hertzberg, S. Filipp, and A. Fuhrer, Effects of surface treatments on flux tunable transmon qubits, *npj Quantum Inf.* **7**, 157 (2021).
- [29] T. Brecht, W. Pfaff, C. Wang, Y. Chu, L. Frunzio, M. H. Devoret, and R. J. Schoelkopf, Multilayer microwave integrated quantum circuits for scalable quantum computing, *npj Quantum Inf.* **2**, 1 (2016).
- [30] C. Axline, M. Reagor, R. Heeres, P. Reinhold, C. Wang, K. Shain, W. Pfaff, Y. Chu, L. Frunzio, and R. J. Schoelkopf, An architecture for integrating planar and 3D cQED devices, *Appl. Phys. Lett.* **109**, 042601 (2016).
- [31] C. Zhou, P. Lu, M. Praquin, T.-C. Chien, R. Kaufman, X. Cao, M. Xia, R. Mong, W. Pfaff, D. Pekker, and M. Hatridge, A modular quantum computer based on a quantum state router, [arXiv:2109.06848](https://arxiv.org/abs/2109.06848).
- [32] A. Gold, J. P. Paquette, A. Stockklauser, M. J. Reagor, M. S. Alam, A. Bestwick, N. Didier, A. Nersisyan, F. Oruc, A. Razavi *et al.*, Entanglement across separate silicon dies in a modular superconducting qubit device, *npj Quantum Inf.* **7**, 142 (2021).
- [33] A. P. Vepsäläinen, A. H. Karamlou, J. L. Orrell, A. S. Dogra, B. Loer, F. Vasconcelos, D. K. Kim, A. J. Melville, B. M. Niedzielski, J. L. Yoder *et al.*, Correlated charge noise and relaxation errors in superconducting qubits, *Nature* **584**, 551 (2020).
- [34] C. D. Wilen, S. Abdullah, N. A. Kurinsky, C. Stanford, L. Cardani, G. D’Imperio, C. Tomei, L. Faoro, L. B. Ioffe, C. H. Liu *et al.*, Correlated charge noise and relaxation errors in superconducting qubits, *Nature* **594**, 369 (2021).
- [35] L. Cardani, F. Valenti, N. Casali, G. Catelani, T. Charpentier, M. Clemenza, I. Colantoni, A. Cruciani, G. D’Imperio, L. Gironi *et al.*, Reducing the impact of radioactivity on quantum circuits in a deep-underground facility, *Nat. Commun.* **12**, 2733 (2021).
- [36] J. M. Boter, J. P. Dehollain, J. P. G. van Dijk, Y. Xu, T. Hensgens, R. Versluis, H. W. L. Naus, J. S. Clarke, M. Veldhorst, F. Sebastiano, and L. M. K. Vandersypen, The spider-web array a sparse spin qubit array, [arXiv:2110.00189](https://arxiv.org/abs/2110.00189).
- [37] Y. Chen, C. Neill, P. Roushan, N. Leung, M. Fang, R. Barends, J. Kelly, B. Campbell, Z. Chen, B. Chiaro *et al.*, Qubit architecture with high coherence and fast tunable coupling, *Phys. Rev. Lett.* **113**, 220502 (2014).
- [38] D. C. McKay, S. Filipp, A. Mezzacapo, E. Magesan, J. M. Chow, and J. M. Gambetta, Universal gate for fixed-frequency qubits via a tunable bus, *Phys. Rev. Appl.* **6**, 064007 (2016).
- [39] F. Yan, P. Krantz, Y. Sung, M. Kjaergaard, D. L. Campbell, T. P. Orlando, S. Gustavsson, and W. D. Oliver, Tunable Coupling Scheme for Implementing High-Fidelity Two-Qubit Gates, *Phys. Rev. Appl.* **10**, 054062 (2018).
- [40] P. S. Mundada, G. Zhang, T. Hazard, and A. A. Houck, Suppression of Qubit Crosstalk in a Tunable Coupling Superconducting Circuit, *Phys. Rev. Appl.* **12**, 054023 (2019).
- [41] P. Zhao, K. Linghu, Z. Li, P. Xu, R. Wang, G. Xue, Y. Jin, and H. Yu, Quantum Crosstalk Analysis for Simultaneous Gate Operations on Superconducting Qubits, *PRX Quantum* **3**, 020301 (2022).
- [42] P. J. Koppinen, L. M. Väistö, and I. J. Maasilta, Complete stabilization and improvement of the characteristics of tunnel junctions by thermal annealing, *Appl. Phys. Lett.* **90**, 053503 (2007).
- [43] J. V. Gates, M. A. Washington, and M. Gurvitch, Critical current uniformity and stability of Nb/Al-oxide-Nb Josephson junctions, *J. Appl. Phys.* **55**, 1419 (1984).
- [44] I. M. Pop, T. Fournier, T. Crozes, F. Lecocq, I. Matei, B. Panetier, O. Buisson, and W. Guichard, Fabrication of stable and reproducible submicron tunnel junctions, *J. Vac. Sci. Technol. B* **30**, 010607 (2012).
- [45] A. Bilmes, A. K. Händel, S. Volosheniuk, A. V. Ustinov, and J. Lisenfeld, In-situ bandaged Josephson junctions for superconducting quantum processors, *Supercond. Sci. Technol.* **34**, 125011 (2021).
- [46] C. E. Murray, Material matters in superconducting qubits, *Materials Science and Engineering: R: Reports* **146**, 100646 (2021).
- [47] M. A. Sillanpää, J. I. Park, and R. W. Simmonds, Coherent quantum state storage and transfer between two phase qubits via a resonant cavity, *Nature (London)* **449**, 438 (2007).
- [48] J. Majer, J. M. Chow, J. M. Gambetta, J. Koch, B. R. Johnson, J. A. Schreier, L. Frunzio, D. I. Schuster, A. A. Houck, A. Wallraff *et al.*, Coupling superconducting qubits via a cavity bus, *Nature (London)* **449**, 443 (2007).
- [49] J. Koch, T. M. Yu, J. Gambetta, A. A. Houck, D. I. Schuster, J. Majer, A. Blais, M. H. Devoret, S. M. Girvin, and R. J. Schoelkopf, Charge-insensitive qubit design derived from the cooper pair box, *Phys. Rev. A* **76**, 042319 (2007).
- [50] M. Göppl, A. Fragner, M. Baur, R. Bianchetti, S. Filipp, J. M.

- Fink, P. J. Leek, G. Puebla, L. Steffen, and A. Wallraff, Coplanar waveguide resonators for circuit quantum electrodynamics, *J. Appl. Phys.* **104**, 113904 (2008).
- [51] D. M. Pozar, *Microwave Engineering* (Wiley, 2011).
- [52] J. Ghosh, A. Galiautdinov, Z. Zhou, A. N. Korotkov, J. M. Martinis, and M. R. Geller, High-fidelity controlled- σ^z gate for resonator-based superconducting quantum computers, *Phys. Rev. A* **87**, 022309 (2013).
- [53] L. H. Pedersen, N. M. Møller, and K. Mølmer, Fidelity of quantum operations, *Phys. Lett. A* **367**, 47 (2007).
- [54] J. M. Martinis and M. R. Geller, Fast adiabatic qubit gates using only σ^z control, *Phys. Rev. A* **90**, 022307 (2014).
- [55] C. J. Wood and J. M. Gambetta, Quantification and characterization of leakage errors, *Phys. Rev. A* **97**, 032306 (2018).
- [56] A. Megrant, C. Neill, R. Barends, B. Chiaro, Y. Chen, L. Feigl, J. Kelly, Erik Lucero, M. Mariantoni, P. J. J. O'Malley *et al.*, Planar superconducting resonators with internal quality factors above one million, *Appl. Phys. Lett.* **100**, 113510 (2012).
- [57] G. Calusine, A. Melville, W. Woods, R. Das, C. Stull, V. Bolkhovsky, D. Braje, D. Hover, D. K. Kim, X. Miloshi *et al.*, Analysis and mitigation of interface losses in trenched superconducting coplanar waveguide resonators, *Appl. Phys. Lett.* **112**, 062601 (2018).
- [58] R. Gao, W. Yu, H. Deng, H.-S. Ku, Z. Li, M. Wang, X. Miao, Y. Lin, and C. Deng, Epitaxial titanium nitride microwave resonators: Structural, chemical, electrical, and microwave properties, *Phys. Rev. Materials* **6**, 036202 (2022).
- [59] M. A. Tremblay, N. Delfosse, and M. E. Beverland, Constant-overhead quantum error correction with thin planar connectivity, [arXiv:2109.14609](https://arxiv.org/abs/2109.14609).
- [60] P. Zhao, D. Lan, P. Xu, G. Xue, M. Blank, X. Tan, H. Yu, and Y. Yu, Suppression of Static ZZ Interaction in an All-Transmon Quantum Processor, *Phys. Rev. Appl.* **16**, 024037 (2021).
- [61] A. Kandala, K. X. Wei, S. Srinivasan, E. Magesan, S. Carnevale, G. A. Keefe, D. Klaus, O. Dial, and D. C. McKay, Demonstration of a High-Fidelity cnot Gate for Fixed-Frequency Transmons with Engineered ZZ Suppression, *Phys. Rev. Lett.* **127**, 130501 (2021).
- [62] J. Johansson, P. Nation, and F. Nori, QuTiP: An open-source Python framework for the dynamics of open quantum systems, *Comput. Phys. Commun.* **183**, 1760 (2012).

Supplementary material for "Tunable coupling of widely separated superconducting qubits: A possible application towards a modular quantum device"

Peng Zhao,^{1,*} Yingshan Zhang,^{1,†} Guangming Xue,^{1,‡} Yirong Jin,¹ and Haifeng Yu¹

¹Beijing Academy of Quantum Information Sciences, Beijing 100193, China

(Dated: May 26, 2022)

Cross-resonance gate

In the main text, we show that the introduced longer-range coupler can be employed for realizing longer-range tunable ZZ coupling and CZ gates by controlling the bus frequency. Here, we further show that the proposed coupler can also be used to implement cross-resonance gates [1]. Cross-resonance (CR) gate is an all-microwave-controlled two-qubit gate, which is realized by driving the control qubit at the frequency of the target qubit, and has been demonstrated as a leading two-qubit gate scheme for qubit architectures with fixed-frequency qubits [2]. One of the major parasitic interactions, that degrade the performance of CR gates, is the parasitic ZZ coupling [1, 3]. Since the implementation of CR gates is based on the transversal (XY) coupling between qubits, it is highly desirable to suppress the parasitic ZZ coupling while keeping adequate XY coupling strength for implementing CR gates [4, 5]. From the point of view of perturbation theory, the XY and ZZ coupling are generally enabled by different virtual transition paths, thus the suppression of ZZ coupling does not always mean that the XY coupling is also suppressed [4]. This suggests that one can maintain the XY interaction while suppressing ZZ coupling, thus XY -interaction-based two-qubit gates, such as iSWAP gates or CR gates, can be realized with ZZ suppression [4, 5].

CX gate

In the following discussion, we will show that CR gates can be realized with ZZ suppression for two qubits coupled via the proposed longer-range coupler (see Fig.2 of the main text). For this system, by setting the bus frequency above 5.5 GHz, the ZZ coupling can be suppressed below 10 kHz (see Fig.3(a) of the main text). Thus, we consider that in the coupled qubit system, the bus takes the fixed frequency at 5.5 GHz, suppressing the parasitic ZZ coupling for implementing CR gates. The resonator coupling strength g is 190 MHz, and other system parameters are the same as in Fig.3(a) of the main text.

Here, we intend to realize CX (CNOT) gate using the CR gate scheme, i.e., driving the control qubit Q_2 at the frequency of the target qubit Q_1 . In addition, besides the CR drive applied to Q_2 , here we consider that an additional cancellation drive is

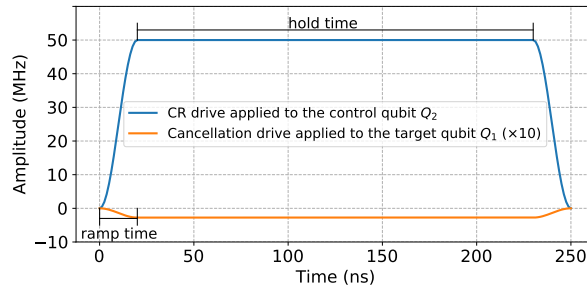


FIG. S1: Typical control pulse with cosine-shaped ramp for implementing CX (CNOT) gates, where the full width at maximum is defined as the hold time.

*Electronic address: shangniguo@sina.com

†Electronic address: zhangys@baqis.ac.cn

‡Electronic address: xuegm@baqis.ac.cn

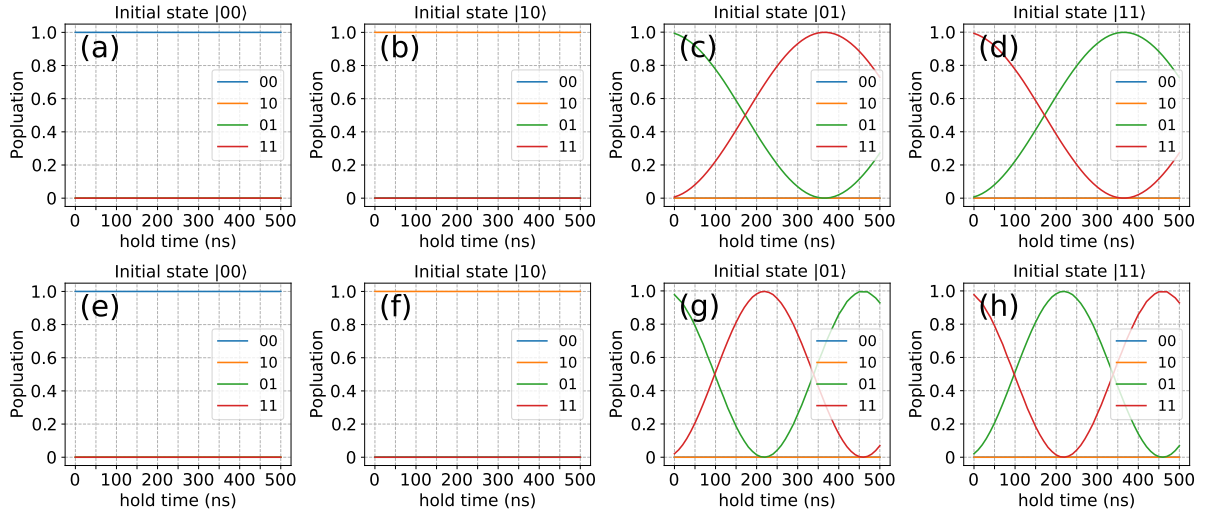


FIG. S2: Populations versus the hold time for four initial states with the CR drive and the cancellation drive applied to Q_2 and Q_1 , respectively. The typical pulse shape is given in Fig. S1. Here, the ramp time is 20 ns. (a-d) the amplitude of the CR drive is $\Omega_2/2\pi = 50$ MHz and the amplitude of the cancellation drive is $\Omega_1 = -0.0054\Omega_2$. (e-h) the amplitude of the CR drive is $\Omega_2/2\pi = 100$ MHz and the amplitude of the cancellation drive is $\Omega_1 = -0.0058\Omega_2$.

applied to Q_1 [2]. The system Hamiltonian under microwave drives can be expressed as

$$H_{full} = H + H_d, \quad H_d = \sum_{i=1,2} \Omega_i (a_i^\dagger + a_i) \cos(\omega_d t), \quad (\text{S1})$$

where H is the undriven system Hamiltonian given in Eq.(1) of the main text, $\Omega_{1(2)}$ denotes the amplitude of the cancellation drive (CR drive) applied to $Q_{1(2)}$, and ω_d is the drive frequency, i.e., the (dressed) frequency of Q_1 .

For the CX gate calibration, the amplitude of the cancellation drive is chosen to ensure no operation on the target qubit Q_1 when the control qubit Q_2 is in state $|0\rangle$ [6]. Thus, up to single-qubit phase compensation (single-qubit phase gate), the CX gate can be implemented by carefully choosing the amplitude of the CR drive and the gate time. The typical pulse shape for the CX gate is shown in Fig. S1, where the pulse has cosine-shaped ramps, and the full width at maximum is defined as the hold time.

Figure S2 shows the qubit population versus the hold time during the gate operations. One can find that with the cancellation drive, there is indeed no operation on Q_1 when Q_2 is in state $|0\rangle$. On the contrary, when Q_2 is in state $|1\rangle$, the population of Q_1 shows a normal Rabi oscillation. Thus, by choosing optimal hold times, CX gates can be obtained.

As shown in Fig. S2(a-d), for a CR drive with $\Omega_2/2\pi = 50$ MHz, a CX gate can be obtained with hold time of 365 ns, and the gate fidelity is 0.9996 [7]. The gate time could be shorter by increasing the CR drive amplitude. For example, as shown in Fig. S2(e-h), where the amplitude is 100 MHz, a CX gate can be achieved with the hold time of 220 ns and the gate fidelity is 0.9988. The increased gate error can be reduced by increasing the ramp time [6]. When increasing the ramp time to 25 ns, a higher-fidelity (0.9996) CX gate can be obtained with the hold time of 213 ns.

-
- [1] J. M. Chow, A. D. Córcoles, J. M. Gambetta, C. Rigetti, B. R. Johnson, J. A. Smolin, J. R. Rozen, G. A. Keefe, M. B. Rothwell, M. B. Ketchen, and M. Steffen, Simple All-Microwave Entangling Gate for Fixed-Frequency Superconducting Qubits, *Phys. Rev. Lett.* **107**, 080502 (2011).
- [2] P. Jurcevic, A. Javadi-Abhari, L. S. Bishop, I. Lauer, D. F. Bogorin, M. Brink, L. Capelluto, O. Günlük, T. Itoko, N. Kanazawa *et al.*, Demonstration of quantum volume 64 on a superconducting quantum computing system, *Quantum Sci. Technol.* **6**, 025020 (2021).
- [3] S. Sheldon, E. Magesan, J. M. Chow, and J. M. Gambetta, Procedure for systematically tuning up cross-talk in the cross-resonance gate, *Phys. Rev. A* **93**, 060302(R) (2016).
- [4] P. Zhao, D. Lan, P. Xu, G. Xue, M. Blank, X. Tan, H. Yu, and Y. Yu, Suppression of Static ZZ Interaction in an All-Transmon Quantum Processor, *Phys. Rev. Appl.* **16**, 024037 (2021).
- [5] A. Kandala, K. X. Wei, S. Srinivasan, E. Magesan, S. Carnevale, G. A. Keefe, D. Klaus, O. Dial, and D. C. McKay, Demonstration of a High-Fidelity cnot Gate for Fixed-Frequency Transmons with Engineered ZZ Suppression, *Phys. Rev. Lett.* **127**, 130501 (2021).
- [6] M. Malekakhlagh and E. Magesan, Mitigating off-resonant error in the cross-resonance gate, [arXiv:2108.03223](https://arxiv.org/abs/2108.03223).

[7] L. H. Pedersen, N. M. Møller, and K. Mølmer, Fidelity of quantum operations, *Phys. Lett. A* **367**, 47 (2007).

